Reproducible NiO/Ga$_2$O$_3$ Vertical Rectifiers with Breakdown Voltage > 8 kV

Jian-Sian Li [1], Hsiao-Hsuan Wan [1], Chao-Ching Chiang [1], Xinyi Xia [1], Timothy Jinsoo Yoo [2], Honggyu Kim [2], Fan Ren [1] and Stephen J. Pearton [2,*]

1   Department of Chemical Engineering, University of Florida, Gainesville, FL 32606, USA;
    jiansianli@ufl.edu (J.-S.L.); hwan@ufl.edu (H.-H.W.); cchiang@ufl.edu (C.-C.C.); xiaxinyi@ufl.edu (X.X.);
    fren@che.ufl.edu (F.R.)
2   Department of Materials Science and Engineering, University of Florida, Gainesville, FL 32606, USA;
    tyoo@ufl.edu (T.J.Y.); honggyukim@ufl.edu (H.K.)
*   Correspondence: spear@mse.ufl.edu

Abstract: Optimized vertical heterojunction rectifiers with a diameter of 100 μm, consisting of sputter-deposited p-type NiO forming a p–n junction with thick (10 μm) Ga$_2$O$_3$ drift layers grown by halide vapor phase epitaxy (HVPE) on (001) Sn-doped (10^{19} cm^{-3}) β-Ga$_2$O$_3$ substrates, exhibited breakdown voltages > 8 kV over large areas (>1 cm^2). The key requirements were low drift layer doping concentrations (<10^{16} cm^3), low power during the NiO deposition to avoid interfacial damage at the heterointerface and formation of a guard ring using extension of the NiO beyond the cathode metal contact. Breakdown still occurred at the contact periphery, suggesting that further optimization of the edge termination could produce even larger breakdown voltages. On-state resistances without substrate thinning were <10 mΩ·cm^{-2}, leading to power figure-of-merits > 9 GW·cm^{-2}. The devices showed an almost temperature-independent breakdown to 600 K. These results show the remarkable potential of NiO/Ga$_2$O$_3$ rectifiers for performance beyond the limits of both SiC and GaN. The important points to achieve the excellent performance were: (1) low drift doping concentration, (2) low power during the NiO deposition and (3) formation of a guard ring.

Keywords: gallium oxide; power electronics; rectifier

1. Introduction

The ultra-wide bandgap semiconductors with bandgaps > 4.5 eV include BN, diamond, AlN and Ga$_2$O$_3$. These materials have the potential for much higher voltage operation than the currently available SiC and GaN power devices, but with lower on-resistance and switching losses. Ga$_2$O$_3$ appears to be an attractive option because of the availability of low cost, large area crystals. The various polytypes of Ga$_2$O$_3$ are attracting attention for their potential application in power switching, solar-blind UV detectors and lateral transistors with enhanced two-dimensional electron gases densities. It is possible to grow bulk crystals of the stable monoclinic β-polymorph from the melt, which enables large-diameter, high-quality substrates for homoepitaxy with low manufacturing costs. The rhombohedral α-polymorph has the largest bandgap and is isomorphous with α-Al$_2$O$_3$, so it is grown on inexpensive sapphire substrates. The orthorhombic κ-polymorph possesses ferroelectric properties and large spontaneous electrical polarization.

Ga$_2$O$_3$ has a high critical electric field strength—at least 8 mV·cm^{-1}. This allows for higher operating voltages and lower switching losses in power electronics. Ga$_2$O$_3$ devices switch faster than Si devices at the same voltage and current ratings. The large bandgap makes it promising for high temperatures and radiation environment applications. As a result, Ga$_2$O$_3$ is being considered for several power electronics applications, including inverters, motor drives and power supplies. There is particular interest in kV-class vertical

rectifiers for use in electric vehicles and their charging infrastructure as well as power management systems for improved switching efficiency for next generation power grids and efficiently interfacing renewable energy sources with these grids [1–4]. Power conversion systems that convert electricity from one form to another comprise AC-to-AC, AC-to-DC, DC-to-AC and DC-to-DC converters, which are used to adjust the voltages and currents for specific applications. A typical example of an electric vehicle and its charging system requires these essential components of power switching and conditioning. A key aspect is the boost converter, which takes in an input voltage and outputs a higher voltage at the load terminals. The key to this operation is a power switch. The enhancement of the efficiency of these switches leads to a much higher efficiency conversion and also to improved system compactness.

One of the goals is to achieve a high-power figure of merit for power electronic devices, defined as $(V_B)^2/R_{ON}$ where V_B is the reverse breakdown voltage and R_{ON-} is the on-state resistance [1–4]. To achieve a high-power figure of merit, a rectifier must have a low drift layer concentration, with high electron mobility, as well as low R_{ON}, and optimized edge termination to prevent current crowding [1,5–21]. The breakdown voltage is larger for thicker drift layers, but this degrades on-resistance. To achieve a low Ron, a thin drift layer with high electron mobility is required. In addition, vertical geometry devices are desirable, because of their higher power conversion efficiency and absolute currents compared to lateral devices [1,3–5]. The expression for R_{ON} is $R_{ON} = \left(4V_B^2\right)/\varepsilon\mu E_C^3$, where ε is the permittivity, μ is the mobility and E_C is the critical field for breakdown. The latter scales approximately as $E_G^{1.7}$. The critical field decreases with the drift layer doping and is doping-dependent at large thickness.

The lack of p-type doping options for Ga_2O_3 has led to the use of p-type oxides to form p–n heterojunctions with the n-type Ga_2O_3 [6–14]. The most successful has been NiO, deposited by sputtering. The forward current transport mechanism in such junctions is typically by recombination at low biases and trap-assisted tunneling at higher bias [10,21–26]. Promising rectifier performance has been reported with this approach [12–14,21–39], including $V_B > 8$ kV, with a figure of merit of 13.2 GW·cm^{-2} [12]. The rationale for this current work is to use a p–n heterojunction to achieve a higher breakdown voltage than is possible with Schottky rectifiers.
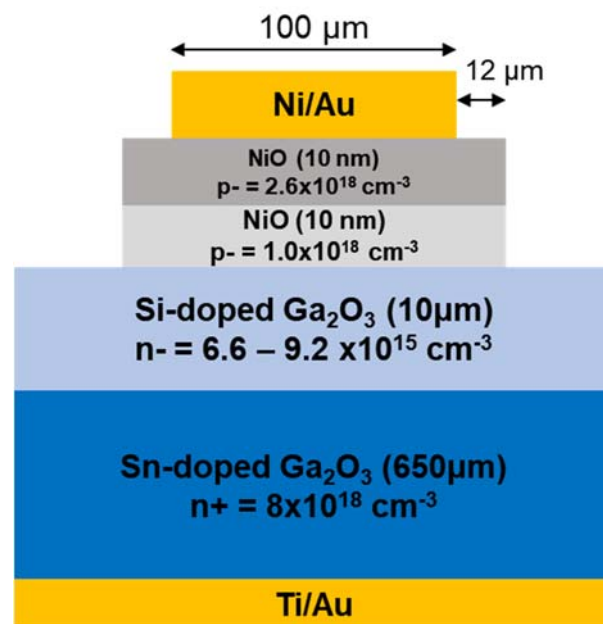
Optimization of the heterojunction rectifier device structure is crucial to achieve both high V_B and low R_{ON}, as well as providing management of the maximum electric fields within the structure to enhance further the device voltage blocking capability [40–45]. The design variables include the thickness and doping of the layers, doping in the drift layer and the use of the NiO as a guard ring by extending it beyond the metal cathode [46–62]. In this paper, we report an investigation of the uniformity of achieving high V_B and low R_{ON} in heterojunction rectifiers, the effect of drift layer doping and the temperature dependence of the performance of NiO/Ga_2O_3 to 600 K.

2. Experimental Section

Vertical geometry Schottky rectifiers and NiO/Ga_2O_3 rectifiers were fabricated on the same wafers to compare the characteristics. The bilayer NiO thickness of 10/10 nm and the length of the NiO extension beyond the cathode contact (12 μm) to form guard rings were held constant. The epitaxial layer structures were purchased from Novel Crystal Technology, Japan. They consisted of a lightly doped drift layer on a conducting substrate. The drift region thickness was 10 μm, grown by halide vapor phase epitaxy (HVPE) on a (001) Sn-doped (10^{19} cm^{-3}), β-Ga_2O_3 single crystal substrate. Both on-resistance and the breakdown voltage increase with the drift layer thickness, but breakdown voltage is a strong function of the epilayer doping and should be as low as possible.

Full area Ohmic contacts were made to the rear surface using Ti/Au deposited by e-beam evaporation and annealed at 550 °C for 180 s under N_2. The front surface was cleaned by UV/Ozone exposure for 15 min. The NiO bilayer was deposited by rf (13.56 MHz) magnetron sputtering at 3mTorr. The hole concentration was adjusted using the Ar/O_2

ratio and the structure was annealed at 300 °C under O_2. The gas flow ratio controls the stoichiometry of the film and the concentration of point defects that define the effective carrier concentration. A very detailed report of the properties of NiO deposited on Ga_2O_3 has been given previously [63]. The layers are polycrystalline, but we have no information on the possible grain boundary effects on the device performance. Finally, a cathode contact of 20/80 nm Ni/Au (100 μm diameter) was deposited onto the NiO layer. The NiO was extended 12 μm beyond the contact metal to form a guard ring. C^{-2}-V plots for the drift layer doping showed the carrier concentration of the drift layers varied from 8×10^{15} to 6.7×10^{15} cm^{-3}. Figure 1 shows a schematic of the heterojunction devices fabricated. We also included Schottky rectifiers without the NiO in order to compare the performance of conventional and heterojunction rectifiers. We note that the NiO extension beyond the top contact was held constant at 12 μm to form a guard ring, which was determined by TCAD simulations to provide the best field mitigation.


Figure 1. Schematic of NiO heterojunction rectifiers fabricated on Ga_2O_3 substrate.

Characterization of the atomic structure of the NiO/β-Ga_2O_3 heterostructure was carried out using high-angle annular dark-field (HAADF) imaging in the scanning mode of transmission electron microscopy (STEM). For STEM studies, cross-section samples were prepared using a Thermo Scientific Helios G4 Cxe dual-beam plasma focused ion beam scanning electron microscope (PFIB-SEM). HAADF imaging in STEM was performed using a Thermo Scientific Themis Z equipped with a probe aberration corrector operated at the acceleration voltage of 200 kV.

The current density–voltage (J–V) characteristics were measured on a Tektronix 370-A curve tracer, 371-B curve and Agilent 4156C. For the highest reverse voltages, a Glassman power supply was employed. The reverse breakdown voltage was defined as the bias for a reverse current reaching 0.1 A·cm^2. The high bias measurements were performed in Fluorinert atmosphere. The devices did not suffer permanent damage at this condition but increasing the voltage a further 50–200 V led to permanent failure through breakdown at the contact periphery. The on-resistance values were calculated assuming the current spreading length was 10 μm and a 45° spreading angle. We also subtracted the resistance of the cable, probe and chuck, which was around 10 Ohm. The drift layer doping was extracted from capacitance–voltage (C–V) data measured at 100 kHz. Photos of the setup have appeared previously [21,38].

3. Results

Figure 2a displays a HAADF-STEM image of the vertical rectifier near the junction between NiO and β-Ga$_2$O$_3$, imaged along the [0$\bar{1}$0] projection with respect to the monoclinic β-Ga$_2$O$_3$ structure. The high-magnification HAADF-STEM image in Figure 2b from the red box in Figure 2a shows that the NiO/β-Ga$_2$O$_3$ interface is atomically abrupt. A 2 nm thick top layer of β-Ga$_2$O$_3$ shows diffuse image intensity of individual atomic columns which is likely due to the local atomic replacement resulting from the NiO sputtering process. However, the atomic structure retains as β-phase with no visible extended defects, indicating that the low-power sputtering process adopted in this study induces negligible structural damage at the surface of β-Ga$_2$O$_3$ compared to previous reports that used higher sputtering powers. Figure 2c,d shows a high-magnification HAADF-STEM image of β-Ga$_2$O$_3$ and a corresponding atomic model which reveal the [0$\bar{1}$0] zone axis with the growth surface of (001).
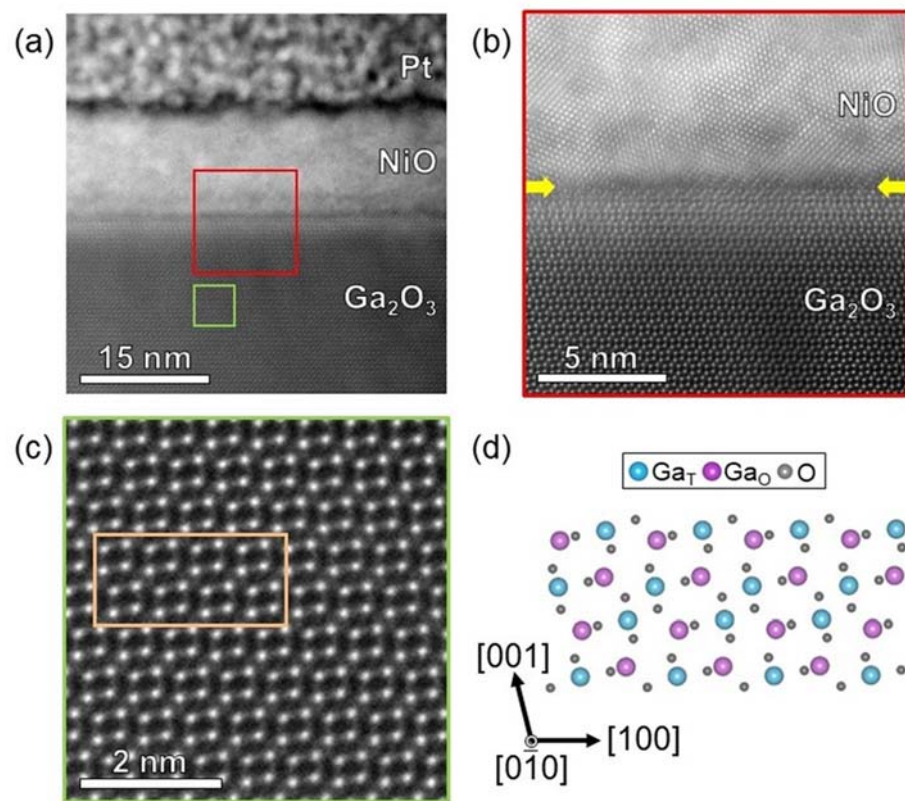
Figure 2. (**a**) HAADF-STEM image of the vertical heterojunction rectifier near the NiO/β-Ga$_2$O$_3$ interface. (**b**) High-magnification HAADF-STEM of the NiO/β-Ga$_2$O$_3$ interface in the red box in (**a**) showing atomically abrupt interface marked with the yellow arrows. (**c**) HAADF-STEM image from the box in (**a,d**) atomic structure of β-Ga$_2$O$_3$ in the box in (**c**), the [0$\bar{1}$0] zone axis with the growth in (001) direction. Blue and purple circles in (**d**) represents Ga atoms with tetrahedral and octahedral coordination, respectively, while grey circles indicate oxygen. Note since the atomic number sensitive image contracts in HAADF-STEM images, only Ga atomic columns are seen in (**c**).

Figure 3 shows how important it is to have the lowest possible ion energy during the sputtering process in order to minimize the damage to the semiconductor surface. The top of Figure 3 shows the presence of a disordered region when using a power of 150 W, corresponding to a negative self-bias of 95–100 V on the powered electrode. By sharp contrast, when the power was lowered to 70 W, the bottom of Figure 3 shows that the disorder was significantly reduced. This rf sputtering power corresponded to a self-bias of 60–70 V, which reduced the corresponding ion energy incident on the surface and therefore reduced the ion-induced damage. We found this was crucial in achieving high breakdown

voltages in the heterojunction rectifiers. The Ga_2O_3 surface was sensitive to disruption and under plasma etching conditions, the damage depth could reach over 100 nm unless careful attention was paid to the minimization of ion-induced damage.
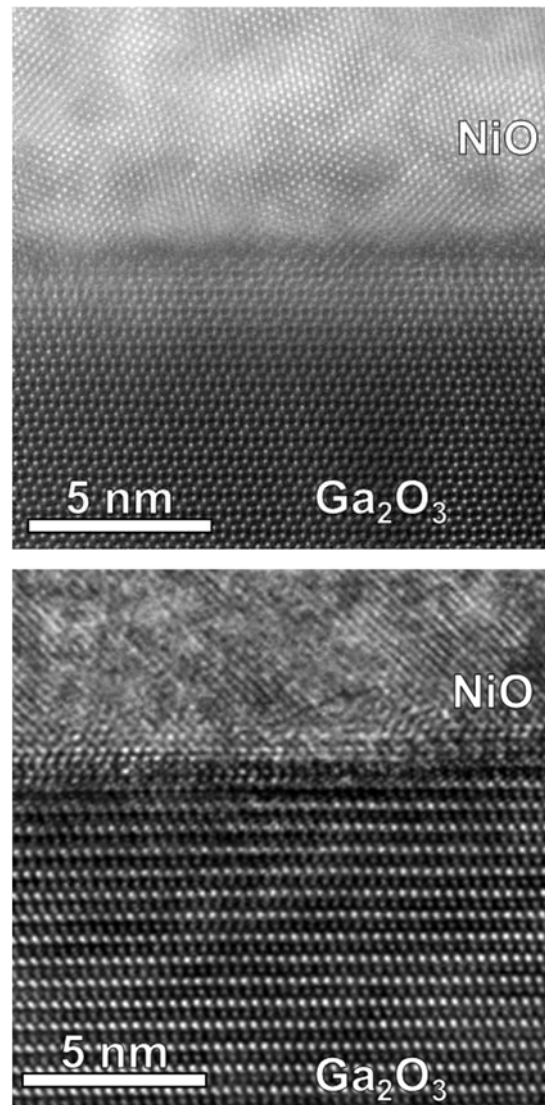

Figure 3. Cross-sectional TEM images for the interfaces of NiO/Ga_2O_3 = heterojunctions with the NiO deposited at 150 W sputtering power(**top**) or 70 W (**bottom**). The top image was recorded along the [0$\bar{1}$0] zone axis bottom image was recorded along the [100] projection with respect to β-Ga_2O_3.

Figure 4 shows an optical image of the devices fabricated over an approximate 1 cm^2 area. We measured 24 separate devices over this area to give an idea of uniformity. We focused on the 100 μm devices. The devices fell at the edge of the top contact due to field-induced breakdown. The rectifiers that failed often showed delamination of the epitaxial layer. There were also multiple crack lines observed along the [0$\bar{1}$0] direction. The low thermal conductivity of Ga_2O_3 produced mechanical failure of the material along the natural cleavage planes. The concentration of heat in the lightly doped epitaxial layer relative to the heavily doped substrate led to differential thermal expansion and delamination of the epitaxial layer.
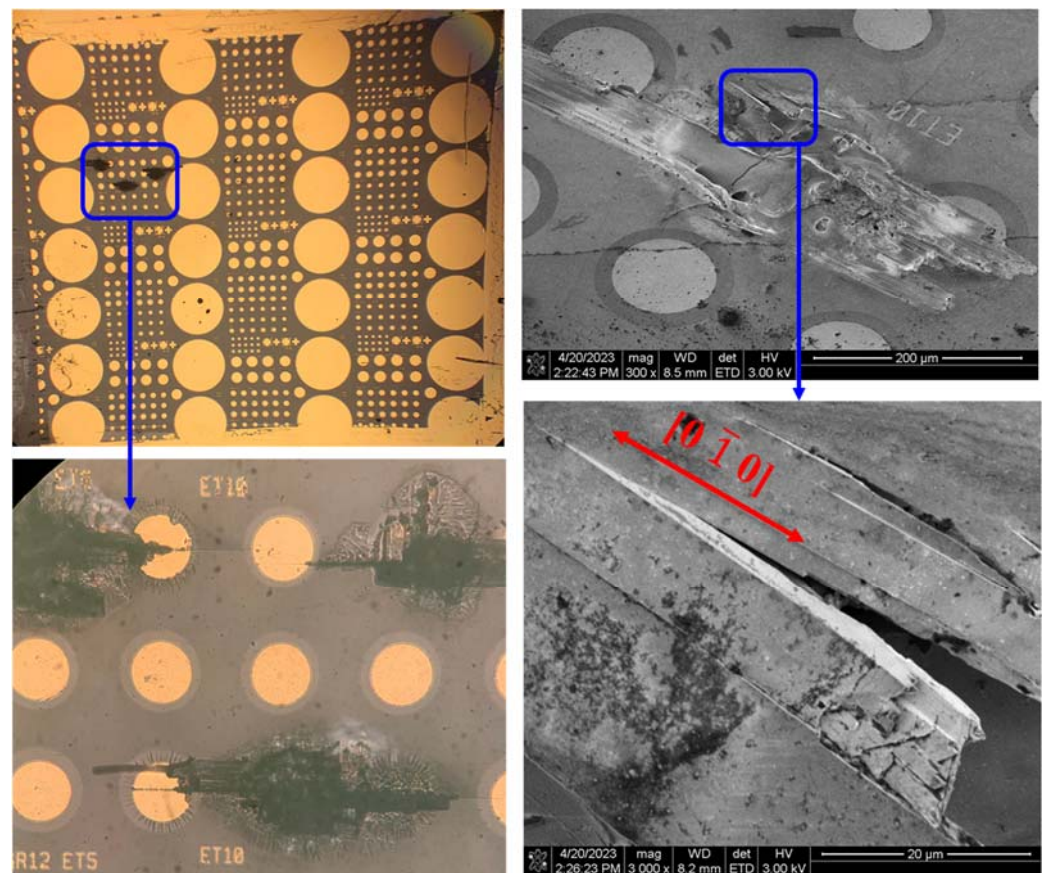
Figure 4. Optical image of devices in a 1 cm^2 area that was used to quantify uniformity of device parameters (**top left**). Devices tested to failure showed catastrophic breakdown at the contact periphery (**bottom left**) and delamination along crystal planes (**right**, **top** and **bottom**).

Figure 5 shows the collected C^{-2}-V data from 24 locations. The drift layer doping varied in the range 6.6–9.2 $\times$ 10^{15} cm^{-2} over the 1 cm^{-2} area. This was outstanding uniformity from an HVPE growth cycle.
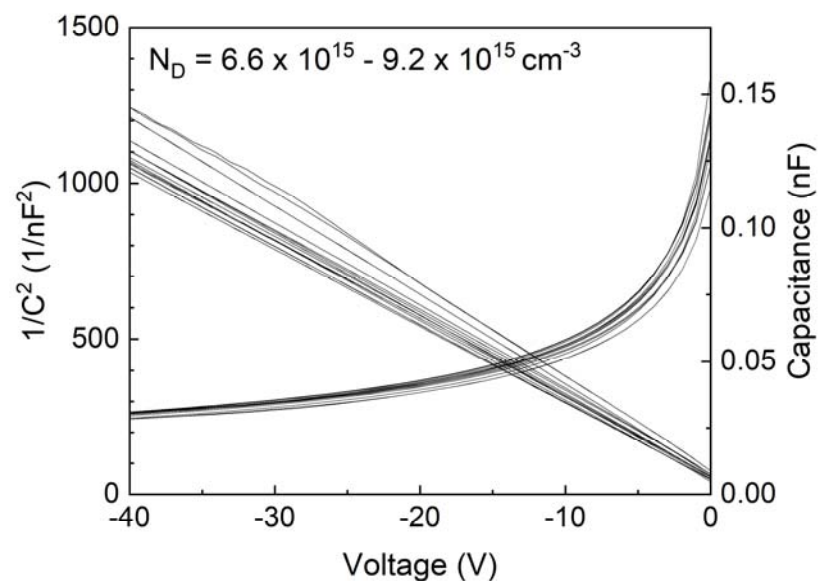

Figure 5. C^{-2}-V plots from 24 devices with a 1 $\times$ 1 cm^2 area on the fabricated wafer.

Figure 6 shows a compilation of forward I–V characteristics from the 24 devices, along with the corresponding R_{ON} and on–off ratios. The former varied in the range 7.1–7.8 mΩ·cm^2 and the on–off ratios were in the range from 4.8×10^{11} to 2.9×10^{12}. The turn-on voltages were derived from the linear plots of forward current density as a function of voltage and are shown in Figure 7. These were tightly distributed in the range 2.1–2.2 V.
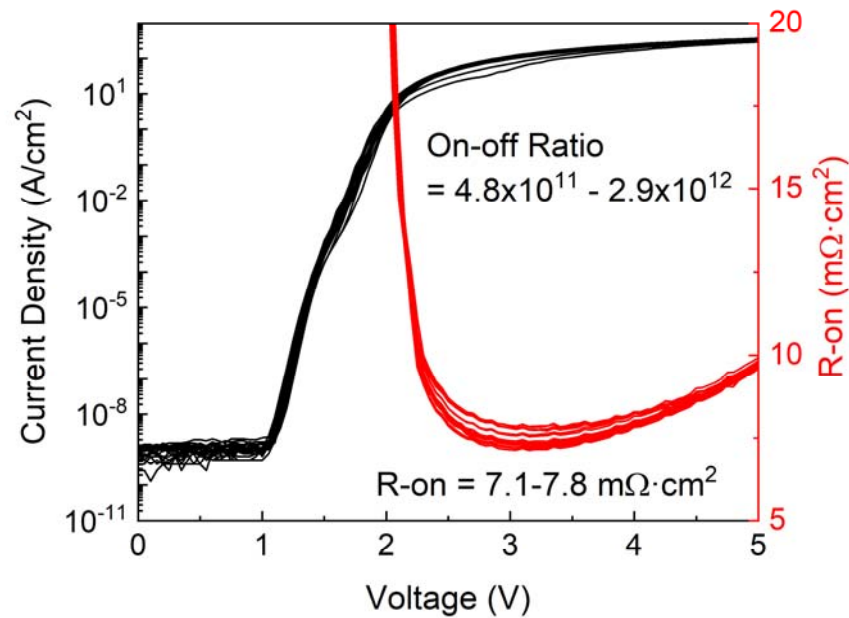

Figure 6. Compilation of forward I–V characteristics from 24 devices measured over a 1 cm^2 area. The corresponding range of R_{ON} and on–off ratios are also shown.
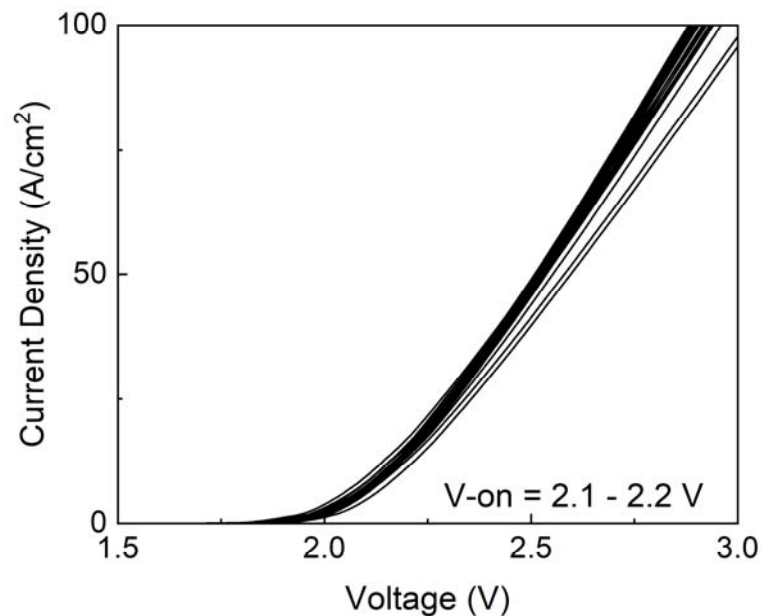
Figure 7. Linear pots of J–V from which the forward turn-on voltages were calculated.

Figure 8 shows a collection of the reverse I–V characteristics from the 24 different devices measured. The distribution of the V_B values, defined as the voltage where the reverse current reaches 0.1 A·cm^{-2}, showed that most were >8 kV. By contrast, the Schottky rectifiers fabricated on the same regions had V_B values of 1100–1500 V, showing the advantage of using the heterojunction approach. When the drift layer doping was higher (8×10^{15} cm^{-3}), the V_B values were centered around 7.5 kV, confirming the importance

of low background carrier concentration. Typically, the Schottky rectifier results in the literature are in the range 800–2 kV for planar devices at these epi thicknesses, but there is a strong variation from wafer-to-wafer and the position on the wafer due to existing uniformity issues.
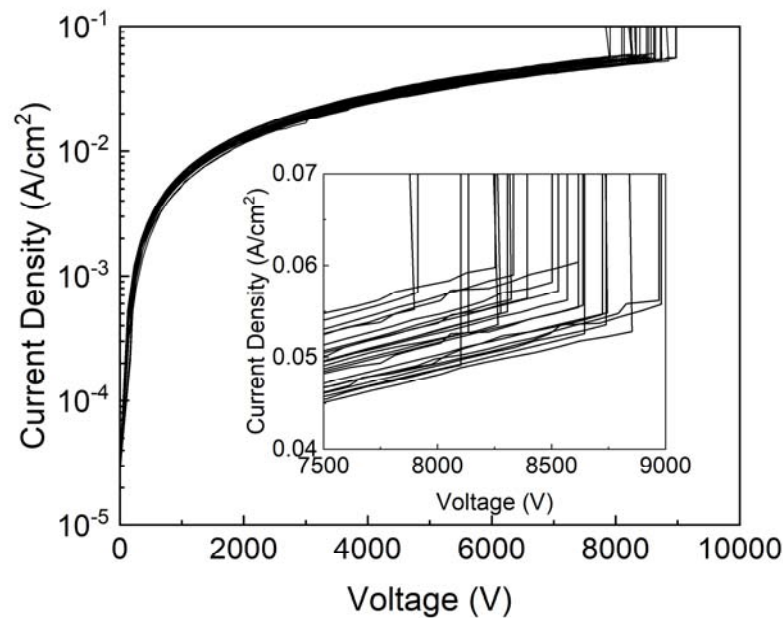
Figure 8. Reverse current density-voltage plots for heterojunction rectifiers fabricated over 1 cm^2 area. The inset shows an expanded view of the breakdown region.

A more detailed view is shown in the inset of Figure 8, with 22 of the 24 devices showing breakdown > 8 kV. The maximum V_B was 8.9 kV. These results emphasized the excellent uniformity of the starting epitaxial layers. When breakdown occurred, it was still at the contact periphery, with delamination of the epilayers occurring, as shown in the images in Figure 4 (left bottom and right, top and bottom). This indicates that field crowding at the edge of the contact remains an issue.

The reverse current densities at −100 V are shown in Figure 9 for the population of devices measured. Again, the spatial variation was relatively small, with all devices exhibiting values <10^{-7} A·cm^{-2}.

We also measured the temperature dependence of V_B. Figure 10 shows that for the heterojunction devices, there was a relatively small degradation in V_B to 600 K. This was in contrast to the case of the Schottky rectifiers fabricated on the same wafers, where the breakdown voltage exhibited a large negative temperature coefficient. We also observed that the R_{ON} increased with temperature, due to the deterioration of mobility. In Ga$_2$O$_3$, the ionization energy of the n-type dopants is small, so increased ionization does not reduce the R_{ON}. Note that in the figure we have shown the range of values obtained at 300 K; we took the highest value for discussion of the temperature dependence.

To place this work in context, Figure 11 shows a compilation of the literature values for on-resistance as a function of the breakdown voltage for the rectifiers measured at room temperature, along with the theoretical values for SiC, GaN and Ga$_2$O$_3$. The bar indicated in red shows the values we obtained in this work for the breakdown voltage of the NiO/GaO$_3$ rectifiers as a function of temperature from 300 = −600 K. Note that the heterojunction rectifiers have much larger breakdown voltages than the Schottky diodes. Since this was the first study of the temperature dependence in the performance of the heterojunction rectifiers, more work is needed to understand the results, but the large bandgaps of the NiO and Ga$_2$O$_3$ are conducive to high temperature operation. In addition, while impact ionization should have a positive temperature coefficient, that is not the

dominant breakdown mechanism in the current state-of-the art material, where the impact ionization of deep acceptors has been identified as the dominant mechanism [64,65].
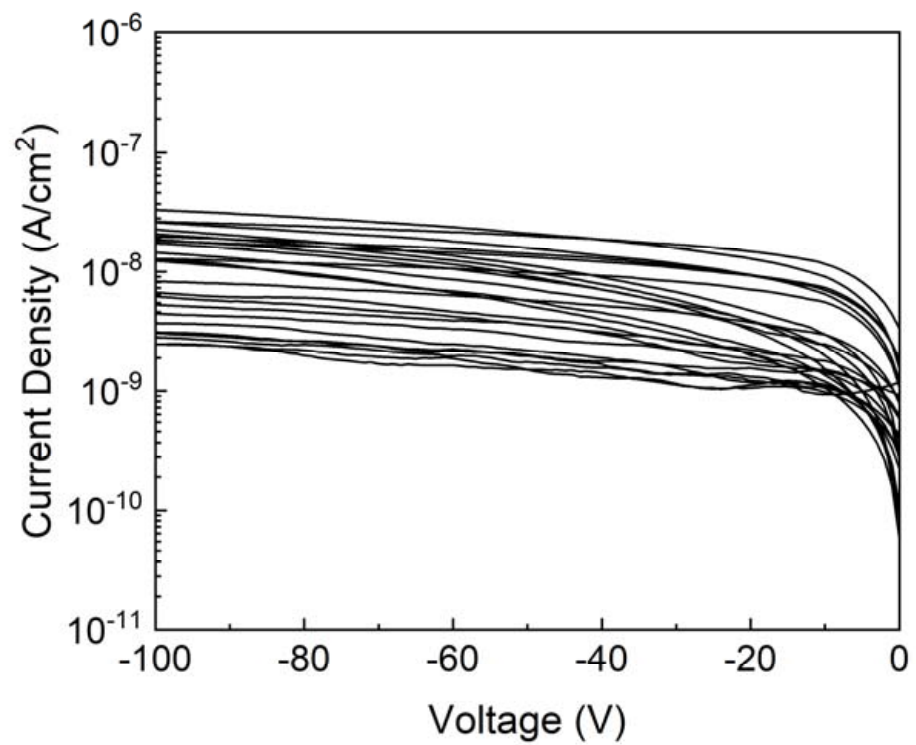

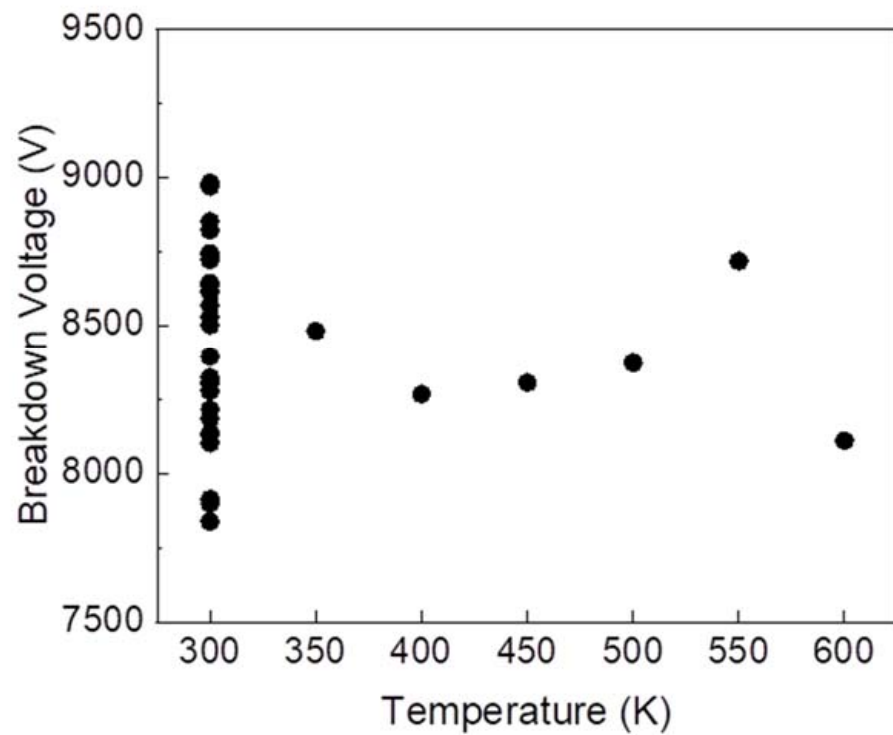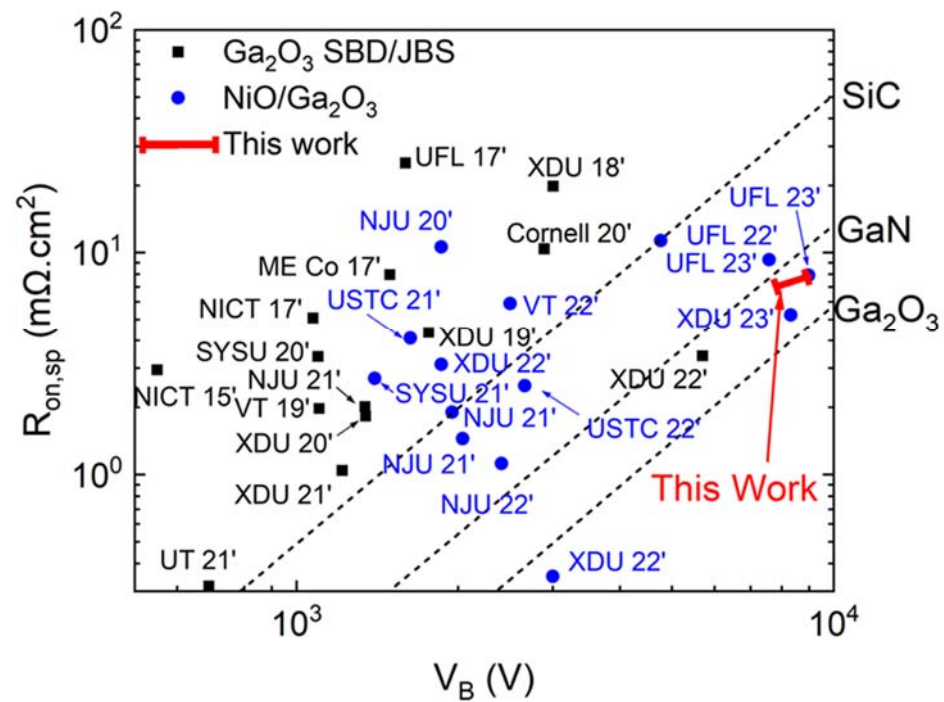**Figure 9.** Reverse J-V characteristics to −100 V from 24 devices.

Figure 10. Temperature dependence of breakdown voltage in heterojunction rectifiers. The range of values at 300 K is also shown.

Figure 11. Compilation of Ron versus V_B of conventional Schottky Barrier Diodes and Junction Barrier Schottky diodes (SBD/JBS) and NiO/Ga_2O_3 heterojunction small area rectifiers reported in the literature. The results from this manuscript in the temperature range 300–600 K are shown in red as the bar. The other results are all from room temperature measurements.

4. Summary and Conclusions

The power figure of merits reported here were around 26% of the theoretical maximum for Ga_2O_3 assuming the 1D punch-through breakdown mechanism; it is anticipated that the continued reduction in defect density could enhance the future performance closer to this maximum. This is because bulk Ga_2O_3 crystals are known to have internal planar defects, i.e., plate-like voids and stacking faults, and it is known that higher dislocation densities lead to higher leakage currents in Ga_2O_3 rectifiers. The dislocations can act as recombination centers for electrons and holes, leading to an increased probability of carrier recombination and subsequent leakage current and hence lower breakdown voltage. The killer defect density was still quite high (10~100/cm^2), caused by a specific powder mainly generated during epitaxial deposition. One possible approach to removing these is to soak the sample in 100 °C 11 M KOH for 30 min to remove it. It should be an important step for fabricating larger diodes. The difficulty of having a thicker epilayer is due to the formation of cracks that occur during longer growth times.

The NiO/Ga_2O_3 heterojunction rectifier is potentially an ideal structure for high-voltage and high-power applications, where it can offer better efficiency and reduced energy losses compared to traditional semiconductors. The wide bandgap of both NiO (~3.9 eV) and β-Ga_2O_3 (4.8 eV) also makes the power rectifiers from this heterojunction attractive for high-temperature applications. The heterojunction produced breakdown voltages far more than the Schottky rectifiers fabricated on the same wafer and confirmed that the NiO can act as both the p-layer and guard ring material. For a particular drift layer doping, there is a saturation thickness beyond which V_B does not increase further. If the doping level is reduced, the saturation thickness increases. In our case, we observed a clear increase in the V_B with reduced drift layer doping. It was also important to minimize the R_{ON} to limit the power lost due to Joule heating. It should also be remembered that the R_{ON} is not necessarily the heterojunction rectifiers actual resistance in the on-state, where the conduction mechanism is dominated by the minority carrier diffusion of minority carriers.

The R_{ON} normally reported is the unipolar drift resistance, which is usually smaller than the diffusion resistance.

What are the implications for the expected critical breakdown field of Ga_2O_3? This is generally reported as ~8 mV·cm^{-1}, but there is considerable uncertainty around this value, since most calculations assume breakdown occurs when the applied electric field and depletion width are sufficiently high to create infinite charge multiplication. This inherently assumes that the impact ionization is the breakdown mechanism, but this has never been experimentally verified in Ga_2O_3 and in any case, the impact ionization coefficients have not been measured either. The performance of $NiO/\beta\text{-}Ga_2O_3$ rectifiers deteriorates only slightly with temperature up to 600 K. Thermal-induced failure of rectifiers can occur due to plastic crystallographic deformation near the epi–substrate interface, and electrical breakdown is still dominated by field crowding at the contact periphery [66].

The important points to achieve high device performance were: (1) low drift doping concentration, (2) low power during the NiO deposition and (3) formation of a guard ring. The functional dependence of the first of these is well understood, but it has not been widely understood that the surface of Ga_2O_3 is quite sensitive too ion-induced damage, hence, the NiO sputter depiction conditions must be optimized. Finally, field mitigation at the edge of the top contact is still crucial, hence, the NiO extension beyond this contact is important.

The excellent performance reported here make the NiO/Ga_2O_3 power rectifiers promising for high-power and high-temperature applications such as electric vehicles, power electronics and aerospace.

Author Contributions: All contributed equally to all aspects of paper. All authors have read and agreed to the published version of the manuscript.

Data Availability Statement: The data that supports the findings of this study are available within the article.

Conflicts of Interest: The authors have no conflict of interest to disclose.

References

1. Kokubun, Y.; Kubo, S.; Nakagomi, S. All-oxide p–n heterojunction diodes comprising p-type NiO and n-type β-Ga_2O_3. *Appl. Phys. Express* **2016**, *9*, 091101. [CrossRef]
2. Wang, C.; Zhang, J.; Xu, S.; Zhang, C.; Feng, Q.; Zhang, Y.; Ning, J.; Zhao, S.; Zhou, H.; Hao, Y. Progress in state-of-the-art technologies of Ga_2O_3 devices. *J. Phys. D Appl. Phys.* **2021**, *54*, 243001. [CrossRef]
3. Pearton, S.; Ren, F.; Tadjer, M.; Kim, J. Perspective: Ga_2O_3 for ultra-high power rectifiers and MOSFETS. *J. Appl. Phys.* **2018**, *124*, 220901. [CrossRef]
4. Green, A.J.; Speck, J.; Xing, G.; Moens, P.; Allerstam, F.; Gumaelius, K.; Neyer, T.; Arias-Purdue, A.; Mehrotra, V.; Kuramata, A.; et al. β-Gallium oxide power electronics. *APL Mater.* **2022**, *10*, 029201. [CrossRef]
5. Lu, X.; Deng, Y.; Pei, Y.; Chen, Z.; Wang, G. Recent advances in NiO/Ga_2O_3 heterojunctions for power electronics. *J. Semicond.* **2023**, *44*, 061802.
6. Galazka, Z. Growth of bulk β-Ga_2O_3 single crystals by the Czochralski method. *J. Appl. Phys.* **2022**, *131*, 031103. [CrossRef]
7. Wong, M.H.; Higashiwaki, M. Vertical β-Ga_2O_3 power transistors: A review. *IEEE Trans. Electron Devices* **2020**, *67*, 3925–3937. [CrossRef]
8. Nouketcha, F.L.; Cui, Y.; Lelis, A.; Green, R.; Darmody, C.; Schuster, J.; Goldsman, N. Investigation of wide-and ultrawide-bandgap semiconductors from impact-ionization coefficients. *IEEE Trans. Electron Devices* **2020**, *67*, 3999–4005. [CrossRef]
9. Dong, P.; Zhang, J.; Yan, Q.; Liu, Z.; Ma, P.; Zhou, H.; Hao, Y. 6 kV/3.4 mΩ cm^2 Vertical β-Ga_2O_3 Schottky Barrier Diode With BV 2/R on, sp Performance Exceeding 1-D Unipolar Limit of GaN and SiC. *IEEE Electron Device Lett.* **2022**, *43*, 765–768. [CrossRef]

10. Zhang, J.; Dong, P.; Dang, K.; Zhang, Y.; Yan, Q.; Xiang, H.; Su, J.; Liu, Z.; Si, M.; Gao, J.; et al. Ultra-wide bandgap semiconductor Ga_2O_3 power diodes. *Nat. Commun.* **2022**, *13*, 3900. [CrossRef]

11. Sharma, S.; Zeng, K.; Saha, S.; Singisetti, U. Field-plated lateral Ga_2O_3 MOSFETs with polymer passivation and 8.03 kV breakdown voltage. *IEEE Electron Device Lett.* **2020**, *41*, 836–839. [CrossRef]

12. Gong, H.; Chen, X.; Xu, Y.; Chen, Y.; Ren, F.; Liu, B.; Gu, S.; Zhang, R.; Ye, J. Band alignment and interface recombination in NiO/β-Ga_2O_3 Type-II pn heterojunctions. *IEEE Trans. Electron Devices* **2020**, *67*, 3341–3347. [CrossRef]

13. Xia, X.; Li, J.-S.; Chiang, C.-C.; Yoo, T.J.; Ren, F.; Kim, H.; Pearton, S. Annealing temperature dependence of band alignment of NiO/β-Ga_2O_3. *J. Phys. D Appl. Phys.* **2022**, *55*, 385105. [CrossRef]

14. Pintor-Monroy, M.I.; Barrera, D.; Murillo-Borjas, B.L.; Ochoa-Estrella, F.J.; Hsu, J.W.; Quevedo-Lopez, M.A. Tunable electrical and optical properties of nickel oxide (NiO x) thin films for fully transparent $NiOx$–Ga_2O_3 p–n junction diodes. *ACS Appl. Mater. Interfaces* **2018**, *10*, 38159–38165. [CrossRef]

15. Deng, Y.; Yang, Z.; Xu, T.; Jiang, H.; Ng, K.W.; Liao, C.; Su, D.; Pei, Y.; Chen, Z.; Wang, G.; et al. Band alignment and electrical properties of NiO/β-Ga_2O_3 heterojunctions with different β-Ga_2O_3 orientations. *Appl. Surf. Sci.* **2023**, *622*, 156917. [CrossRef]

16. Lu, X.; Zhou, X.; Jiang, H.; Ng, K.W.; Chen, Z.; Pei, Y.; Lau, K.M.; Wang, G. 1-kV Sputtered p-NiO/n-Ga_2O_3 Heterojunction Diodes with an Ultra-Low Leakage Current Below 1 μA/cm². *IEEE Electron Device Lett.* **2020**, *41*, 449–452. [CrossRef]

17. Xiao, M.; Wang, B.; Liu, J.; Zhang, R.; Zhang, Z.; Ding, C.; Lu, S.; Sasaki, K.; Lu, G.-Q.; Buttay, C.; et al. Packaged Ga_2O_3 Schottky rectifiers with over 60-A surge current capability. *IEEE Trans. Power Electron.* **2021**, *36*, 8565–8569. [CrossRef]

18. Liao, C.; Lu, X.; Xu, T.; Fang, P.; Deng, Y.; Luo, H.; Wu, Z.; Chen, Z.; Liang, J.; Pei, Y.; et al. Optimization of NiO/β-Ga_2O_3 Heterojunction Diodes for High-Power Application. *IEEE Trans. Electron Devices* **2022**, *69*, 5722–5727. [CrossRef]

19. Lv, Y.; Wang, Y.; Fu, X.; Dun, S.; Sun, Z.; Liu, H.; Zhou, X.; Song, X.; Dang, K.; Liang, S.; et al. Demonstration of β-Ga_2O_3 junction barrier Schottky diodes with a Baliga's figure of merit of 0.85 GW/cm² or a 5 A/700 V handling capabilities. *IEEE Trans. Power Electron.* **2020**, *36*, 6179–6182. [CrossRef]

20. Li, W.; Saraswat, D.; Long, Y.; Nomoto, K.; Jena, D.; Xing, H.G. Near-ideal reverse leakage current and practical maximum electric field in β-Ga_2O_3 Schottky barrier diodes. *Appl. Phys. Lett.* **2020**, *116*, 192101. [CrossRef]

21. Sharma, R.; Xian, M.; Fares, C.; Law, M.E.; Tadjer, M.; Hobart, K.D.; Ren, F.; Pearton, S.J. Effect of probe geometry during measurement of >100 A Ga_2O_3 vertical rectifiers. *J. Vac. Sci. Technol. A Vac. Surf. Film.* **2021**, *39*, 013406. [CrossRef]

22. Hu, Z.; Nomoto, K.; Li, W.; Zhang, Z.; Tanen, N.; Thieu, Q.T.; Sasaki, K.; Kuramata, A.; Nakamura, T.; Jena, D.; et al. Breakdown mechanism in 1 kA/cm² and 960 V E-mode β-Ga_2O_3 vertical transistors. *Appl. Phys. Lett.* **2018**, *113*, 122103. [CrossRef]

23. Chabak, K.D.; Leedy, K.D.; Green, A.J.; Mou, S.; Neal, A.T.; Asel, T.; Heller, E.R.; Hendricks, N.S.; Liddy, K.; Crespo, A.; et al. Lateral β-Ga_2O_3 field effect transistors. *Semicond. Sci. Technol.* **2019**, *35*, 013002. [CrossRef]

24. Roy, S.; Bhattacharyya, A.; Ranga, P.; Splawn, H.; Leach, J.; Krishnamoorthy, S. High-k oxide field-plated vertical (001) β-Ga_2O_3 Schottky barrier diode with Baliga's figure of merit over 1 GW/cm². *IEEE Electron Device Lett.* **2021**, *42*, 1140–1143. [CrossRef]

25. Li, J.-S.; Chiang, C.-C.; Xia, X.; Yoo, T.J.; Ren, F.; Kim, H.; Pearton, S. Demonstration of 4.7 kV breakdown voltage in NiO/β-Ga_2O_3 vertical rectifiers. *Appl. Phys. Lett.* **2022**, *121*, 042105. [CrossRef]

26. Gong, H.; Yu, X.; Xu, Y.; Chen, X.; Kuang, Y.; Lv, Y.; Yang, Y.; Ren, F.-F.; Feng, Z.; Gu, S.; et al. β-Ga_2O_3 vertical heterojunction barrier Schottky diodes terminated with p-NiO field limiting rings. *Appl. Phys. Lett.* **2021**, *118*, 202102. [CrossRef]

27. Gong, H.; Zhou, F.; Xu, W.; Yu, X.; Xu, Y.; Yang, Y.; Ren, F.; Gu, S.; Zheng, Y.; Zhang, R.; et al. 1.37 kV/12 A NiO/β-Ga_2O_3 heterojunction diode with nanosecond reverse recovery and rugged surge-current capability. *IEEE Trans. Power Electron.* **2021**, *36*, 12213–12217. [CrossRef]

28. Gong, H.; Chen, X.; Xu, Y.; Ren, F.-F.; Gu, S.; Ye, J. A 1.86-kV double-layered NiO/β-Ga_2O_3 vertical p–n heterojunction diode. *Appl. Phys. Lett.* **2020**, *117*, 022104. [CrossRef]

29. Yan, Q.; Gong, H.; Zhang, J.; Ye, J.; Zhou, H.; Liu, Z.; Xu, S.; Wang, C.; Hu, Z.; Feng, Q.; et al. β-Ga_2O_3 hetero-junction barrier Schottky diode with reverse leakage current modulation and BV2/Ron, sp value of 0.93 GW/cm². *Appl. Phys. Lett.* **2021**, *118*, 122102. [CrossRef]

30. Wang, C.; Gong, H.; Lei, W.; Cai, Y.; Hu, Z.; Xu, S.; Liu, Z.; Feng, Q.; Zhou, H.; Ye, J.; et al. Demonstration of the p-NiO x/n-Ga_2O_3 Heterojunction Gate FETs and Diodes with BV 2/R on, sp Figures of Merit of 0.39 GW/cm² and 1.38 GW/cm². *IEEE Electron Device Lett.* **2021**, *42*, 485–488. [CrossRef]

31. Yan, Q.; Gong, H.; Zhou, H.; Zhang, J.; Ye, J.; Liu, Z.; Wang, C.; Zheng, X.; Zhang, R.; Hao, Y. Low density of interface trap states and temperature dependence study of Ga_2O_3 Schottky barrier diode with p-NiOx termination. *Appl. Phys. Lett.* **2022**, *120*, 092106. [CrossRef]

32. Zhou, F.; Gong, H.; Xu, W.; Yu, X.; Xu, Y.; Yang, Y.; Ren, F.-F.; Gu, S.; Zheng, Y.; Zhang, R.; et al. 1.95-kV beveled-mesa NiO/β-Ga_2O_3 heterojunction diode with 98.5% conversion efficiency and over million-times overvoltage ruggedness. *IEEE Trans. Power Electron.* **2021**, *37*, 1223–1227. [CrossRef]

33. Hao, W.; He, Q.; Zhou, K.; Xu, G.; Xiong, W.; Zhou, X.; Jian, G.; Chen, C.; Zhao, X.; Long, S. Low defect density and small I−V curve hysteresis in NiO/β-Ga_2O_3 pn diode with a high PFOM of 0.65 GW/cm². *Appl. Phys. Lett.* **2021**, *118*, 043501. [CrossRef]

34. Zhou, X.; Liu, Q.; Hao, W.; Xu, G.; Long, S. Normally-off β-Ga_2O_3 Power Heterojunction Field-Effect-Transistor Realized by p-NiO and Recessed-Gate. In Proceedings of the 2022 IEEE 34th International Symposium on Power Semiconductor Devices and ICs (ISPSD), Vancouver, BC, Canada, 22–25 May 2022; pp. 101–104.

35. Hao, W.; Wu, F.; Li, W.; Xu, G.; Xie, X.; Zhou, K.; Guo, W.; Zhou, X.; He, Q.; Zhao, X. High-Performance Vertical β-Ga$_2$O$_3$ Schottky Barrier Diodes Featuring P-NiO JTE with Adjustable Conductivity. In Proceedings of the 2022 International Electron Devices Meeting (IEDM), San Francisco, CA, USA, 3–7 December 2022; pp. 9.5. 1–9.5. 4.

36. Hao, W.; He, Q.; Zhou, X.; Zhao, X.; Xu, G.; Long, S. 2.6 kV NiO/Ga$_2$O$_3$ heterojunction diode with superior high-temperature voltage blocking capability. In Proceedings of the 2022 IEEE 34th International Symposium on Power Semiconductor Devices and ICs (ISPSD), Vancouver, BC, Canada, 22–25 May 2022; pp. 105–108.

37. Li, J.-S.; Chiang, C.-C.; Xia, X.; Ren, F.; Pearton, S. Temperature dependence of on–off ratio and reverse recovery time in NiO/β-Ga$_2$O$_3$ heterojunction rectifiers. *J. Vac. Sci. Technol. A Vac. Surf. Film.* **2022**, *40*, 063407. [CrossRef]

38. Yang, J.; Carey IV, P.; Ren, F.; Chen, Y.-T.; Liao, Y.; Chang, C.-W.; Lin, J.; Tadjer, M.; Pearton, S.; Smith, D.J.; et al. DC and dynamic switching characteristics of field-plated vertical geometry [beta]-Ga$_2$O$_3$ rectifiers. In Proceedings of the Oxide-based Materials and Devices X, San Francisco, CA, USA, 2–7 February 2019; pp. 37–44.

39. Yang, J.; Xian, M.; Carey, P.; Fares, C.; Partain, J.; Ren, F.; Tadjer, M.; Anber, E.; Foley, D.; Lang, A.; et al. Vertical geometry 33.2 A, 4.8 MW cm^2 Ga$_2$O$_3$ field-plated Schottky rectifier arrays. *Appl. Phys. Lett.* **2019**, *114*, 232106. [CrossRef]

40. Wang, B.; Xiao, M.; Spencer, J.; Qin, Y.; Sasaki, K.; Tadjer, M.J.; Zhang, Y. 2.5 kV Vertical Ga$_2$O$_3$ Schottky Rectifier with Graded Junction Termination Extension. *IEEE Electron Device Lett.* **2022**, *44*, 221–224. [CrossRef]

41. Wang, Z.; Gong, H.; Meng, C.; Yu, X.; Sun, X.; Zhang, C.; Ji, X.; Ren, F.; Gu, S.; Zheng, Y.; et al. Majority and Minority Carrier Traps in NiO/β-Ga$_2$O$_3$ p++-n Heterojunction Diode. *IEEE Trans. Electron Devices* **2022**, *69*, 981–987. [CrossRef]

42. Zhou, H.; Zeng, S.; Zhang, J.; Liu, Z.; Feng, Q.; Xu, S.; Zhang, J.; Hao, Y. Comprehensive Study and Optimization of Implementing p-NiO in β-Ga$_2$O$_3$ Based Diodes via TCAD Simulation. *Crystals* **2021**, *11*, 1186. [CrossRef]

43. Wang, Y.; Gong, H.; Lv, Y.; Fu, X.; Dun, S.; Han, T.; Liu, H.; Zhou, X.; Liang, S.; Ye, J.; et al. 2.41 kV Vertical P-Nio/n-Ga$_2$O$_3$ Heterojunction Diodes With a Record Baliga's Figure-of-Merit of 5.18 GW/cm^2. *IEEE Trans. Power Electron.* **2021**, *37*, 3743–3746. [CrossRef]

44. Zhang, J.; Han, S.; Cui, M.; Xu, X.; Li, W.; Xu, H.; Jin, C.; Gu, M.; Chen, L.; Zhang, K.H. Fabrication and interfacial electronic structure of wide bandgap NiO and Ga$_2$O$_3$ p–n heterojunction. *ACS Appl. Electron. Mater.* **2020**, *2*, 456–463. [CrossRef]

45. Ji, M.; Taylor, N.R.; Kravchenko, I.; Joshi, P.; Aytug, T.; Cao, L.R.; Paranthaman, M.P. Demonstration of large-size vertical Ga$_2$O$_3$ Schottky barrier diodes. *IEEE Trans. Power Electron.* **2021**, *36*, 41–44. [CrossRef]

46. Qin, Y.; Wang, Z.; Sasaki, K.; Ye, J.; Zhang, Y. Recent progress of Ga$_2$O$_3$ power technology: Large-area devices, packaging and applications. *Jpn. J. Appl. Phys.* **2023**, *62*, SF0801. [CrossRef]

47. Li, J.S.; Chao, C.; Chso, C.; Xia, X.; Wan, H.H.; Ren, F.; Pearton, S.J. Effect of Drift Layer Doping and NiO Parameters in Achieving 8.7 kV Breakdown in 100 μm Diameter and 4kV/4A in 1mm Diameter NiO/Ga$_2$O$_3$ Rectifiers. *J. Vac. Sci. Technol. A*, 2023; *in press*.

48. Yang, J.; Ren, F.; Tadjer, M.; Pearton, S.J.; Kuramata, A. Ga$_2$O$_3$ Schottky rectifiers with 1 ampere forward current, 650 V reverse breakdown and 26.5 MW·cm^{-2} figure-of-merit. *AIP Adv.* **2018**, *8*, 055026. [CrossRef]

49. Yang, J.; Fares, C.; Elhassani, R.; Xian, M.; Ren, F.; Pearton, S.J.; Tadjer, M.; Kuramata, A. Reverse Breakdown in Large Area, Field-Plated, Vertical β-Ga$_2$O$_3$ Rectifiers. *ECS J. Solid State Sci. Technol.* **2019**, *8*, Q3159–Q3166. [CrossRef]

50. Li, J.S.; Chiang, C.C.; Xia, X.; Wan, H.S.; Ren, F.; Pearton, S.J. 1 mm^2, 3.6 kV, 4.8 A NiO/Ga$_2$O$_3$ Heterojunction Rectifiers. *ECS J. Solid State Sci. Technol.* 2023; *in press*.

51. Islam, Z.; Haque, A.; Glavin, N.; Xian, M.; Ren, F.; Polyakov, A.Y.; Kochkova, A.; Tadjer, M.; Pearton, S.J. In Situ Transmission Electron Microscopy Observations of Forward Bias Degradation of Vertical Geometry β-Ga$_2$O$_3$ Rectifiers. *ECS J. Solid State Sci. Technol.* **2020**, *9*, 055008. [CrossRef]

52. Islam, Z.; Xian, M.; Haque, A.; Ren, F.; Tadjer, M.; Glavin, N.; Pearton, S. In situ observation of β-Ga$_2$O$_3$ Schottky diode failure under forward biasing condition. *IEEE Trans. Electron Devices* **2020**, *67*, 3056–3061. [CrossRef]

53. Sun, R.; Balog, A.R.; Yang, H.; Alem, N.; Scarpulla, M. Degradation of β-Ga$_2$O$_3$ vertical Ni/Au Schottky diodes under forward bias. *IEEE Electron Device Lett.* 2023; *in press*. [CrossRef]

54. Gong, H.; Zhou, F.; Yu, X.; Xu, W.; Ren, F.; Gu, S.; Lu, H.; Ye, J.; Zhang, R. 70-μm-Body Ga$_2$O$_3$ Schottky Barrier Diode With 1.48 K/W Thermal Resistance, 59 A Surge Current and 98.9% Conversion Efficiency. *IEEE Electron Device Lett.* **2022**, *43*, 773–776. [CrossRef]

55. Otsuka, F.; Miyamoto, H.; Takatsuka, A.; Kunori, S.; Sasaki, K.; Kuramata, A. Large-size (1.7 × 1.7 mm^2) β-Ga$_2$O$_3$ field-plated trench MOS-type Schottky barrier diodes with 1.2 kV breakdown voltage and 10^9 high on/off current ratio. *Appl. Phys. Express* **2021**, *15*, 016501. [CrossRef]

56. Hao, W.; Wu, F.; Li, W.; Xu, G.; Xie, X.; Zhou, K.; Zhou, X.; He, Q.; Zhao, X.; Yang, S.; et al. Improved Vertical β-Ga$_2$O$_3$ Schottky Barrier Diodes With Conductivity-Modulated p-NiO Junction Termination Extension. *IEEE Trans. Electron Devices* **2023**, *70*, 2129–2134. [CrossRef]

57. Wei, J.; Wei, Y.; Lu, J.; Peng, X.; Jiang, Z.; Yang, K.; Luo, X. Experimental Study on Electrical Characteristics of Large-Size Vertical β-Ga$_2$O$_3$ Junction Barrier Schottky Diodes. In Proceedings of the 2022 IEEE 34th International Symposium on Power Semiconductor Devices and Ics (ISPSD), Vancouver, BC, Canada, 22–25 May 2022; pp. 97–100.

58. Zhou, F.; Gong, H.H.; Wang, Z.P.; Xu, W.P.; Yu, X.X.; Yang, Y.; Ren, F.F.; Gu, S.L.; Zhang, R.; Zheng, Y.D.; et al. Over 1.8 GW/cm^2 beveled-mesa NiO/β-Ga$_2$O$_3$ heterojunction diode with 800 V/10 A nanosecond switching capability. *Appl. Phys. Lett.* **2021**, *119*, 262103. [CrossRef]

59. Li, J.S.; Chiang, C.C.; Xia, X.; Tsai, C.T.; Ren, F.; Liao, Y.T.; Pearton, S.J. Dynamic Switching of 1.9 A/1.76 kV Forward Current NiO/β-Ga$_2$O$_3$ Rectifiers. *ECS J. Solid State Sci. Technol.* **2022**, *11*, 105003. [CrossRef]

60. Sdoeung, S.; Sasaki, K.; Kawasaki, K.; Hirabayashi, J.; Kuramata, A.; Kasu, M. Characterization of dislocation of halide vapor phase epitaxial (001) β-Ga$_2$O$_3$ by ultrahigh sensitive emission microscopy and synchrotron X-ray topography and its influence on Schottky barrier diodes. *Jpn. J. Appl. Phys.* **2023**, *62*, SF1001. [CrossRef]

61. Wang, B.; Xiao, M.; Knoll, J.; Buttay, C.; Sasaki, K.; Dimarino, C.; Zhang, Y. Low Thermal Resistance (0.5 K/W) Ga$_2$O$_3$ Schottky Rectifiers with Double-Side Packaging. *IEEE Electron Device Lett.* **2021**, *42*, 1132–1134. [CrossRef]

62. Ogawa, K.; Ogawa, N.; Kosaka, R.; Isshiki, T.; Yao, Y.; Ishikawa, Y. Three-Dimensional Observation of Internal Defects in a β-Ga$_2$O$_3$ (001) Wafer Using the FIB–SEM Serial Sectioning Method. *J. Electron. Mater.* **2020**, *49*, 5190–5195. [CrossRef]

63. Nakagomi, S.; Yasuda, T.; Kokubun, Y. Crystal Orientation of Cubic NiO Thin Films Formed on Monoclinic β-Ga$_2$O$_3$ Substrates. Phys. *Phys. Status Solidi B* **2020**, *257*, 1900669. [CrossRef]

64. Li, J.S.; Chiang, C.C.; Xia, X.; Wan, H.H.; Ren, F.; Pearton, S.J. Superior High Temperature Performance of 8 kV NiO/Ga$_2$O$_3$ Vertical Heterojunction Rectifiers. *J. Mater. Chem. C* 2023; *Accepted*. [CrossRef]

65. Yakimov, E.B.; Polyakov, A.Y.; Smirnov, N.B.; Shchemerov, I.V.; Vergeles, P.S.; Yakimov, E.E.; Chernykh, A.V.; Xian, M.; Ren, F.; Pearton, S.J. Role of hole trapping by deep acceptors in electron-beam-induced current measurements in β-Ga$_2$O$_3$ vertical rectifiers. *J. Phys. D Appl. Phys.* **2020**, *53*, 495108. [CrossRef]

66. Xian, M.; Fares, C.; Ren, F.; Islam, Z.; Haque, A.; Tadjer, M.; Pearton, S.J. Asymmetrical Contact Geometry to Reduce Forward-Bias Degradation in β-Ga$_2$O$_3$ Rectifiers. *ECS J. Solid State Sci. Technol.* **2020**, *9*, 035007. [CrossRef]